

Penetrative DNA intercalation and G-base selectivity of an organometallic tetrahydroanthracene Ru^{II} anticancer complex†

Hong-Ke Liu,^{*a} John A. Parkinson,^c Juraj Bella,^e Fuyi Wang^d and Peter J. Sadler^{*b}

Received 20th February 2010, Accepted 6th May 2010

DOI: 10.1039/c0sc00175a

The organometallic Ru^{II} arene complex $[(\eta^6\text{-tha})\text{Ru}(\text{en})\text{Cl}]^+$ (**1**), where tha = tetrahydroanthracene and en = ethylenediamine, is potently cytotoxic towards cancer cells. We have used a combination of HPLC, ESI-MS, 1D- and 2D-NMR, including $[\text{H}, \text{H}]$ ROESY, NOESY, $[\text{H}, \text{N}]$ HSQC (using ^{15}N -**1**), and $[\text{H}, \text{P}]$ experiments to elucidate the role of the non-aromatic, bulky rings of tha in adducts with the DNA hexamer d(CGCCCG), since DNA is a potential target for this drug. Reactions of **1** with single-stranded d(CGCCCG) gave rise to ruthenation at each of the three G bases, whereas reactions of the duplex d(CGCCCG)₂ with 1 mol equiv. **1** led to exclusive ruthenation of G³ and G⁶ (and G⁹, G¹²) and not G² (or G⁸). Addition of a second mol equiv. of **1** gave di-ruthenated adducts (major sites G³/G⁶, G⁶/G⁹, G²/G⁶), and on reaction with a third mol equiv. tri-ruthenation (G², G³/G⁶/G¹²). The NMR data are indicative of the coordinative binding of Ru-tha specifically to G³ and G⁶, together with penetrative intercalation of the bulky non-coordinated tha rings B and C of **1**, selectively between two base pairs G³/C¹⁰:C⁴/G⁹ and G⁶/C⁷:C⁵/G⁸. Intercalation at GpC base steps by tha has a lower energy penalty compared to intercalation at GpG base steps, thereby allowing accommodation of tha. Mono-intercalation of tha reduced the strength of H-bonding between en-NH and GO6. These differences in structural distortions compared to cisplatin induced by the coordinative binding of Ru-tha to GN7 may contribute to the differences in mechanism of action, including protein recognition of the metallated lesions, and lack of cross resistance.

Introduction

There is currently much interest in the design and mechanism of action of ruthenium anticancer complexes.^{1–7} Structural distortions of DNA are thought to play a major role in the anticancer activity of many ruthenium and other transition metal complexes.^{1,8–23} It is apparent that distortions induced in DNA by $[(\eta^6\text{-arene})\text{Ru}(\text{en})\text{Cl}]^+$ organometallic ruthenium(II) arene anticancer complexes^{1,21,24–28} (en = ethylenediamine) differ significantly from those induced by cisplatin.^{9,10} In particular the arene appears to play a significant role in DNA interactions and the cytotoxicity of complexes shows a strong dependence on the arene.^{19,22,23,29,31} The cytotoxic activity of these ruthenium arene complexes appears to increase with the size of the coordinated arene:^{1,24,25} *p*-cymene (Ru-cym) < biphenyl (Ru-bip) < dihydroanthracene (Ru-dha) < tetrahydroanthracene (Ru-tha, **1**,

Fig. 1), the latter complex being as cytotoxic as the clinical platinum drug cisplatin. If the arene is extended, the possibility arises of intercalation between DNA base-pairs. Studies of the interactions of ruthenium complexes Ru-cym and Ru-bip with the 6-mer duplex d(CGCCCG)₂ revealed that the binding of Ru to GN7 is accompanied by strong H-bonding between GO6 and en-NH, and that the arene ligand distorts the duplex either *via* steric interactions (Ru-cym) or *via* intercalation^{19,22,23,32,38} (Ru-bip), which may explain why the IC₅₀ values of complexes Ru-cym and Ru-bip are similar.^{1,24,25} Further work²³ revealed

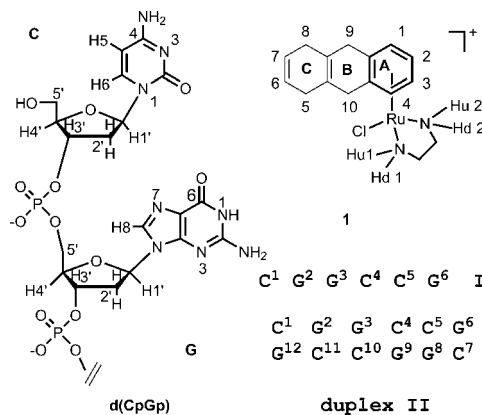


Fig. 1 Structures and NMR numbering schemes for $[(\eta^6\text{-tha})\text{Ru}(\text{en})\text{Cl}]^+$ (**1**) and for the 5'-d(CpGp) fragment of the hexamer d(CGCCCG)₂; single-strand (ss) **I** and duplex **II**.

^aJiangsu Key Laboratory of Biofunctional Materials, School of Chemistry, Nanjing Normal University, Nanjing, China. E-mail: liuhongke@njnu.edu.cn; Tel: +86-2585891651

^bDepartment of Chemistry, University of Warwick, Gibbet Hill Road, Coventry, UK CV4 7AL. E-mail: P.J.Sadler@warwick.ac.uk; Fax: +44-2476523819; Tel: +44-2476523818

^cWestCHEM Department of Pure and Applied Chemistry, University of Strathclyde, 295 Cathedral Street, Glasgow, UK G1 1XL

^dBeijing National Laboratory for Molecular Sciences, Institute of Chemistry, Chinese Academy of Sciences, Beijing, 100190, China

^eSchool of Chemistry, University of Edinburgh, King's Buildings, West Mains Road, Edinburgh, UK EH9 3JJ

† Electronic supplementary information (ESI) available: Reactions of **II** with ^{15}N -**1**, HPLC, HPLC-ESI-MS, NMR and pH measurements, Tables S1–S7 and Figs. S1–S7. See DOI: 10.1039/c0sc00175a

a unique mode of binding of Ru-bip to a 14-mer DNA duplex: the monofunctional fragment $\{(\eta^6\text{-biphenyl})\text{Ru}(\text{en})\}^{2+}$ is highly specific for GN7, although mobile at elevated temperature (migrating to other G residues). The uncoordinated phenyl ring of bip can be involved in π - π stacking with DNA bases either *via* classical intercalation^{19,35–38} between the bases, or with a partially extruded T base.^{23,39,40}

Arene–base stacking may play a role in determining the rates of reactions of Ru^{II} arene complexes with DNA, as appears to be the case for mononucleotides. We have shown previously that the *tha* and *bip* arenes can exert slightly different effects on the chemical reactivity of these Ru^{II} complexes and on distortions induced in DNA.^{26,29,30} For example the rate of reaction of Ru-bip with cGMP is *ca.* 2× slower than that of **1**,²⁷ but Ru-bip induces similar unwinding of DNA as complex **1** (14°).²⁶ Both of these complexes can potentially intercalate into DNA, leading to “downstream” effects on DNA processing and repair mechanisms. Ru-bip is an aromatic intercalator,^{22,23,41} in which all the protons of the extended ring are within the aromatic plane, and can form π - π interactions with bases; however, the extended rings B and C of *tha* in **1** are bulky non-aromatic groups; the three rings A, B and C are not in the same plane and the H5,8 and H9,10 protons are located above or below the arene ring plane by nearly 0.9 Å. The extended rings B and C cannot form π - π interactions with bases in the same way that aromatic intercalators do and so Ru-*tha* is more sterically demanding than Ru-bip. It is reasonable to predict that the intercalative interactions between duplex DNA and Ru-*tha* or Ru-bip should be quite different. The Ru-*tha* complex **1** is 10 times more toxic to cancer cells than Ru-bip.^{24,25}

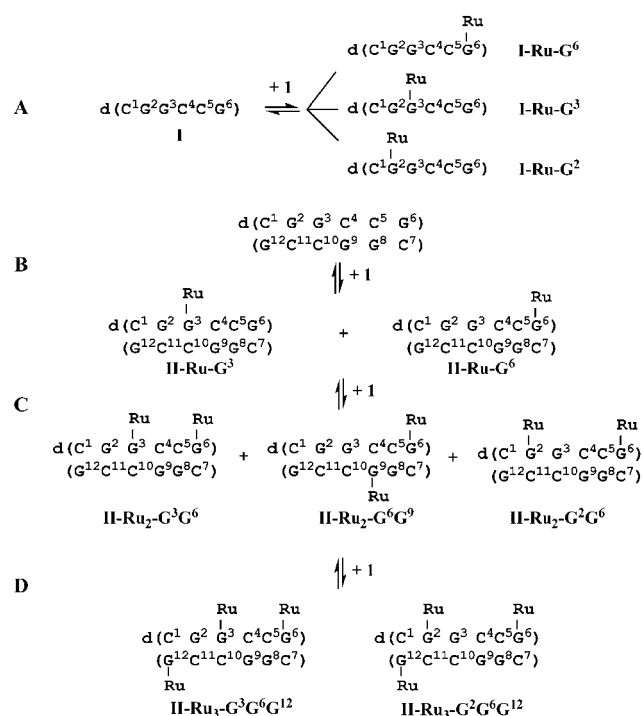
Bulky substituents at the sites of DNA lesions may activate nucleotide-excision repair;^{42,43} however, reports of intercalation by bulky molecules are rare. Gomez-Pinto *et al.*⁴⁴ have shown that intercalation of a modified nucleotide containing a cholesterol derivative into a DNA decamer induces DNA distortions which are different from those induced by aromatic intercalators.^{45,46}

Threading intercalation has attracted recent attention because the intercalator occupies and interacts strongly with both the minor and major grooves of DNA simultaneously. This has been observed for polyaromatic intercalators,^{47–49} dinuclear metallointercalators,^{50–53} and platinum complexes with aromatic side-arms, such as acridine-9-ylthiourea.^{54–56} As a result, threading intercalative interactions promise high DNA binding affinity and specificity, a slow rate of dissociation, and an enhanced ability to block DNA–protein interactions.^{50,57}

It is important to understand the mode of interaction between $[(\eta^6\text{-tha})\text{Ru}(\text{en})\text{Cl}]^+$ (**1**) and DNA since a major contributor to its high potency appears to be the lack of repair of the lesions formed on DNA by this complex,²⁹ *i.e.* lack of recognition by repair enzymes. In the present work we have investigated the role of the extended non-aromatic bulky *tha* in interactions of $[(\eta^6\text{-tha})\text{Ru}(\text{en})\text{Cl}]^+$ (**1**) with the single-stranded hexamer d(CG GCCG) and double-stranded duplex d(CG GCCG)₂ using a wide variety of experimental techniques including HPLC, ESI-MS and 1D ¹H and 2D [¹H, ¹H] ROESY, NOESY, [¹H, ¹⁵N] HSQC (using ¹⁵N-**1**), and [¹H, ³¹P] NMR spectroscopy.

Results

Scheme 1 indicates the reaction pathways that were followed during the course of this study. HPLC enabled separation of single DNA strands even for reactions of the duplex. The 1 : 1, 2 : 1 and 3 : 1 **I**/**I** mixtures, 1.1 : 1 and 2 : 1 **I**/**II** mixtures were studied by HPLC and ESI-MS, and 1.1 : 1, 2 : 1 and 3 : 1 **I**/**II** mixtures were studied by 1D ¹H and 2D [¹H, ¹H] TOCSY NMR experiments. The 1.1 : 1 **I**/**II** mixture was studied by 1D ¹H, 2D ¹⁵N-decoupled [¹H, ¹H] ROESY, NOESY, ¹⁵N-edited [¹H, ¹H] TOCSY and NOESY, 2D ¹⁵N-decoupled [¹H, ¹⁵N] and [¹H, ³¹P] HSQC NMR experiments using ¹⁵N-en labelled **1**. A near-complete NMR spectral assignment of the NOESY NMR spectrum of the 1.1 : 1 **I**/**II** mixture was achieved, although its complexity precluded full structure determination. Assignments were made possible by the known selectivity of **1** for guanines, and the localization of structural perturbations to residues close to the ruthenated G residue. Thus, sequential assignments along each strand always led to cross-peaks largely identical to those of the non-ruthenated duplex. Despite extensive overlap of NOE cross-peaks, little ambiguity in the assignments of individual resonances was found, with cross-validation of signal assignments from related connectivities being possible, with the help of [¹H, ³¹P] HSQC, [¹H, ¹⁵N] HSQC and ¹⁵N-edited [¹H, ¹H] NOESY



Scheme 1 (A) Reaction of single-stranded (ss) hexamer **I** (0.1 mM) with 1 mol equiv. of **1** in H₂O, 310 K for 48 h, gives three mono-ruthenated **I** (**I**-Ru-G², **I**-Ru-G³, **I**-Ru-G⁶). (B) Reaction of double-stranded (ds) hexamer **II** (0.3 mM, 0.1 M NaClO₄) with 1.1 mol equiv. of **1** in 90% H₂O/10% D₂O gives rise to two mono-ruthenated duplexes **II**-Ru-G³ and **II**-Ru-G⁶ as products. Addition of a second mol equiv. of **1** results in di-ruthenated duplexes, including **II**-Ru₂-G³G⁶, **II**-Ru₂-G⁶G⁹ and **II**-Ru₂-G²G⁶ as main products. Addition of a third mol equiv. of **1** results in two tri-ruthenated duplexes **II**-Ru₃-G³G⁶G¹² and **II**-Ru₃-G²G⁶G¹² as main products. Ru = $\{(\eta^6\text{-tha})\text{Ru}(\text{en})\}^{2+}$, **I'**. For structure of **1**, see Fig. 1.

experiments and HPLC-MS data. 2D ^{15}N -decoupled ^1H , ^1H ROESY and NOESY and ^{15}N -decoupled ^1H , ^{15}N HSQC NMR data were also acquired for 2 : 1 and 3 : 1 **I/II** mixtures, but the spectra were too complex for interpretation.

HPLC and ESI-MS characterization of products from ss-DNA **I** + **I**

A 100 μM aqueous solution of **I** was incubated with **I** at 310 K at Ru : **I** molar ratios of 1 : 1, 2 : 1 and 3 : 1 for 48 h in the dark, and these were then analyzed by HPLC. The low ionic strength (5.1×10^{-4} M) ensures that this self-complementary oligonucleotide remains largely single-stranded (calculated melting temperature 264 K) under these conditions.⁵⁸ New peaks were observed for each reaction (Fig. 2 and Table S1 \dagger), and the adducts associated with them were identified subsequently by ESI-MS. The peaks for the observed negative ions are listed in Table S1. \dagger Reaction at a Ru : **I** molar ratio of 1 : 1 resulted in three mono-ruthenated products together with three di-ruthenated products. Reaction at a Ru : **I** molar ratio of 2 : 1 resulted in three di-ruthenated products together with a tri-ruthenated

product. Reaction at a Ru : **I** molar ratio of 3 : 1, gave only one main HPLC peak corresponding to a tri-ruthenated product.

HPLC and ESI-MS characterization of products from reaction of duplex **II** + **I**

An aqueous solution of **I** was incubated with duplex **II** in 0.1 M NaClO_4 at ambient temperature for 24 h at a Ru : **II** molar ratio of 1.1 : 1 in an NMR tube in the dark. This gave rise to HPLC peaks which were identified by ESI-MS as ss-DNA **I** and two mono-ruthenated single-stranded products (see Fig. 2(d), Table S1 \dagger), with relative peak area ratios of 2 : 1. Another equimolar amount of **I** was then added to give a Ru : **II** molar ratio of 2 : 1, and was kept at ambient temperature in the dark for 48 h. This gave HPLC peaks which were identified by ESI-MS as two mono-ruthenated and two di-ruthenated single-stranded products (see Fig. 2(e) and Table S1 \dagger).

NMR characterization of products

Assignments of the ^1H NMR peaks for the ruthenated DNA duplexes were made on the basis of established methods developed for studying right-handed B-DNA duplexes by NMR spectroscopy.⁵⁹ The assignments of the ^1H NMR resonances of free DNA duplex **II** have been reported by Lam and Au-Yeung⁶⁰ and the ^1H and ^{31}P chemical shifts are listed in Table S2. \dagger Terminal (3') base resonance assignments were identified from NOESY NMR data sets and were based on ordering of the $\text{H}2'$ and $\text{H}2''$ proton chemical shifts ($\text{H}2' > \text{H}2''$). The resonance assignments of backbone ^{31}P and sugar ring ^1H ($\text{H}4'$ and $\text{H}3'$) resonances for free and mono-ruthenated DNA duplexes were achieved by ^1H , ^{31}P HSQC NMR experiments⁶¹ and the $\text{H}4'_n$ and $\text{H}3'_{n-1}$ protons were assigned by correlation to their respective $^{31}\text{P}_n$ resonances. The assignments of ruthenated $\text{G}^*\text{H}8$ and $\text{I}'\text{-en-NH}_2$ (NHu and NHd , see Fig. 1 for labelling) resonances of mono-ruthenated DNA duplexes were achieved by reference to 2D ^1H , ^{15}N HSQC and ^{15}N -edited ^1H , ^1H NOESY NMR data. The NMR chemical shifts of the ^1H and ^{31}P resonances associated with these two mono-ruthenated duplex adducts are listed in Table S3 (**II-Ru-G³**), Table S4 (**II-Ru-G⁶**) and Table S2 (free **II**). \dagger The assignments of $\text{H}1,4$, $\text{H}2,3$, $\text{H}9,10$, $\text{H}5,8$, $\text{H}6,7$ and $\text{I}'\text{-en-NH}_2$ (NHu and NHd , see Fig. 1 for labelling) ^1H NMR resonances of $\{(\eta^6\text{-tha})\text{Ru}(\text{en})\}^{2+}$ (**I'**) were achieved by 2D ^1H , ^{15}N HSQC, ^{15}N -edited ^1H , ^1H NOESY and ^1H , ^1H NOESY experiments^{27,28} and are listed in Table 1 and Fig. 5. The assignments of $\text{H}2,3$ and $\text{H}1,4$ NMR resonances of **I'** were achieved by correlations to the $\text{I}'\text{-en-NHu}$ resonances in ^1H , ^1H NOESY NMR data, where the $\text{H}9,10$ protons were assigned by correlation to the $\text{H}1,4$ resonances, and $\text{H}5,8$ protons by correlation to the $\text{H}9,10$ and $\text{H}6,7$ resonances.^{27,28}

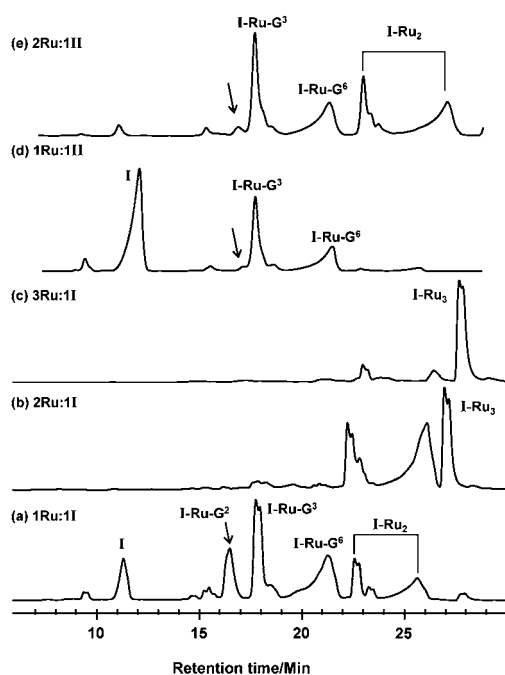


Fig. 2 HPLC chromatograms for reaction of $\{(\eta^6\text{-tha})\text{Ru}(\text{en})\text{Cl}\}^+$ (**I**) with single-stranded (ss) $\text{d}(\text{CGGCCG})$ (**I**) (0.1 mM in H_2O) at Ru : **I** mol ratios of (a) 1 : 1, (b) 2 : 1, and (c) 3 : 1, and for reaction of **I** with duplex $\text{d}(\text{CGGCCG})_2$ (**II**) (0.34 mM, 0.1 M NaClO_4 , 90% $\text{H}_2\text{O}/10\%$ D_2O) at a Ru : **II** mol ratio of (d) 1.1 : 1 and (e) 2 : 1. The mono-ruthenated duplex **II-Ru₁** elutes as mono-ruthenated ss-DNA **I** (**I-Ru-G³** and **I-Ru-G⁶**; species **I-Ru-G³** and **I-Ru-G⁹** are identical, as are **I-Ru-G⁶** and **I-Ru-G¹²**); di-ruthenated duplex **II-Ru₂** elutes as mono-ruthenated ss-DNA **I** (**I-Ru-G³** and **I-Ru-G⁶**, see (d)), and di-ruthenated ss-DNA **I** (**I-Ru₂**, see (e)). It is notable that **G²** is readily ruthenated for single strand **I** (see **I-Ru-G²** in (a)) but not for duplex **II** in (d). Little ruthenation on **G⁸** was observed when 1 mol equiv. of **I** was added to mono-ruthenated duplexes **II-Ru-G³** and **II-Ru-G⁶** (e). Ru = $\{(\eta^6\text{-tha})\text{Ru}(\text{en})\}^{2+}$ (**I'**), and is bound to $\text{G}^{\text{N}7}$ or $\text{G}^{\text{6}7}$; for DNA sequence, see Fig. 1 and Scheme 1.

NMR of 1.1 : 1, 2 : 1 and 3 : 1 **I/II** reactions

Fig. S1 shows the imino and aromatic region of the 800 MHz 1D ^1H NMR spectrum of DNA duplex **II** in the absence (Fig. S1A \dagger) and presence of 1 mol (Fig. S1B \dagger), 2 mol (Fig. S1C \dagger) and 3 mol (Fig. S1D \dagger) equiv. of **I**. Reaction with 1.1 mol equiv. of **I** resulted in the formation of a number of new peaks for **II** (especially near 8.5 ppm ($\text{G}^*\text{H}8$), 13.0–13.6 ppm (imino) and

Table 1 ^1H NMR chemical shifts for $\{[\eta^6\text{-tha}]\text{Ru}(\text{en})(\text{Cl})\}^+$ (**I**) and bound fragment $\{[\eta^6\text{-tha}]\text{Ru}(\text{en})\}^{2+}$ (**I'**) in the 1.1 : 1 **I/II** reaction product **I'-II**, in Ru-tha-9EtG (**I'-9EtG**)^{a,b} and Ru-tha-5'GMP (**I'-GMP**) adducts^{a,b}

Complex	$\delta(^1\text{H})$ ($\Delta\delta$)							
	en-CH ₂	NHd	H1,4	H2,3	NHu	H5,8	H9,10	H6,7
I	2.23/2.43	3.60/3.71	5.50	5.61	6.19/6.29	2.62	3.18	5.75
I'-II ^e	2.34/2.45 (0.11) ^c	3.86/3.95 ^d (0.26/0.24) ^c	6.04 (0.54) ^c	5.97 (0.36) ^c	6.47/6.56 (0.18/0.27) ^c	2.74 (0.12) ^c	4.18 (1.00) ^c	5.84 (0.09) ^c
I'-9EtG ^{b,f}	2.07/2.40 (-0.16) ^h	na	5.85 (0.35) ^h	6.24 (0.63) ^h	na	2.55 (-0.07) ^h	3.20	5.66 (-0.09) ^h
I'-GMP ^{b,g}	2.10/2.40 (-0.13) ⁱ	na	6.16 (0.66) ⁱ	6.16 (0.55) ⁱ	na	3.12 (0.50) ⁱ	4.01 (0.83) ⁱ	5.65 (-0.10) ⁱ

^a For atom labels, see Fig. 1 and Scheme 1. ^b Ref. 28. ^c $\Delta\delta = \delta(\text{I}'\text{-II}) - \delta(\text{I})$ (≥ 0.04 ppm). ^d This assignment is based on a NOESY experiment. ^e At 283 K. ^f At 339 K. ^g At 318 K. ^h $\Delta\delta = \delta(\text{I}'\text{-9EtG}) - \delta(\text{I})$ (≥ 0.04 ppm). ⁱ $\Delta\delta = \delta(\text{I}'\text{-GMP}) - \delta(\text{I})$ (≥ 0.04 ppm).

6.3–6.7 ppm (NHu-**I'**, **I'** is the bound complex **I**, $\{[\eta^6\text{-tha}]\text{Ru}(\text{en})\}^{2+}$, Fig. S1B†). Two imino ^1H NMR resonances were shifted to low-field by +0.04 ppm (G^{3*} , mono-ruthenated G^3 base) and +0.14 ppm (G^9), and two imino ^1H resonances were shifted to high-field by -0.07 ppm (G^{6*} , mono-ruthenated G^6 base) and -0.04 ppm (G^{12}), relative to the free duplex **II** (Figs. S1 and S2, Tables S3, S4 and S2†). Reaction of the second mol equiv. of **I** with the mono-ruthenated duplexes resulted in a notable increase in intensities of the new peaks, especially $\text{G}^*\text{H}8$ (near 8.5 ppm), NHu-**I'** (6.3–6.7 ppm), H5 and H1' resonances; the intensities of imino and H8, H6 resonances of free **II** all decreased (Fig. S1C†). Reaction of the third mol equiv. of **I** with the di-ruthenated duplexes resulted in an increase in the intensities of new peaks, e.g. at 8.8 ppm (Fig. S1D†). The resonances of CH5, CH6, H1' and $\text{G}^*\text{H}8$ moved to low field by up to +0.3 ppm, and the peaks for imino protons almost disappeared.

2D [^1H , ^1H] TOCSY NMR of 1.1 : 1, 2 : 1 and 3 : 1 **I/II** reactions

The 2D TOCSY NMR spectrum of the 1.1 : 1 **I/II** reaction mixture clearly showed the existence of cross-peaks for the two mono-ruthenated duplexes, as seen for example in the aromatic region in Fig. 3B. Two sets of H5-H6 cross-peaks were detected for C^4 , C^5 , C^7 and C^{10} residues. The proportions of Ru-**IIa** and Ru-**IIb** at 283 K were determined by integration of the TOCSY cross-peak volumes of $\text{C}^4\text{-H}5/\text{C}^4\text{-H}6$ of Ru-**IIa**, and $\text{C}^5\text{-H}5/\text{C}^5\text{-H}6$ of Ru-**IIb**, and the HPLC peak areas for **I**-Ru- G^3 and **I**-Ru- G^6 (see Fig. 2d). This gave a Ru-**IIa** : Ru-**IIb** ratio of 2 : 1 ($\pm 10\%$). Other species account for less than 10% of the total DNA. The 2D TOCSY NMR spectrum of the 2 : 1 **I/II** reaction mixture shows that peaks for other new species are present but not all can be assigned due to the complexity of the spectrum (Fig. 3C). It was notable that the intensities of the CH5-CH6 cross-peaks for C^5/C^{11} residues of free **II** decreased remarkably, but those of the CH5-CH6 cross-peaks for $\text{C}^{1'}$, $\text{C}^{4'}$ and $\text{C}^{5'}$ residues of the ruthenated species increased markedly. The 2D TOCSY NMR spectrum of the 3 : 1 **I/II** reaction mixture shows that the CH5-CH6 cross-peaks for C^5/C^{11} residues of free **II** almost completely disappeared (Fig. 3D).

2D [^1H , ^{15}N] HSQC NMR of the 1.1 : 1 **I/II** reaction

These experiments allowed detection of NMR peaks specifically for the $\{[\eta^6\text{-tha}]\text{Ru}(\text{en})\}^{2+}$ fragment. These are commonly difficult to resolve in normal ^1H NMR experiments. One major new species was detected by 2D [^1H , ^{15}N] HSQC NMR analysis

of the 1.1 : 1 mixture of duplex **II** and ^{15}N -**I** (the ^{15}N -en labelled complex **I**) at 283 K in 90% $\text{H}_2\text{O}/10\%$ D_2O (Fig. S3†). Peaks were assignable to en-NHu resonances (the NH protons oriented

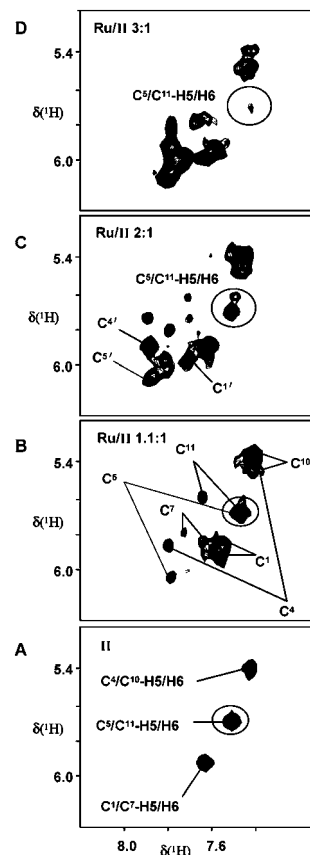


Fig. 3 2D [^1H , ^1H] TOCSY NMR spectrum in the cytosine H5/H6 cross-peak region for free duplex **II** (A), 1.1 : 1 **I/II** mixture (B), 2 : 1 **I/II** mixture (C) and 3 : 1 **I/II** mixture (D) of ruthenium complex **I** and duplex **II** (0.34 mM, 0.1 M NaClO_4) in 90% $\text{H}_2\text{O}/10\%$ D_2O at 283 K. Note that 2 sets of resonances are observed for the C^4 , C^5 , C^7 and C^{10} residues, suggesting the presence of two mono-ruthenated products in the 1.1 : 1 **I/II** mixture (B). Significant changes are observed for H5/H6 resonances of C^5 and C^{11} bases when the Ru:**II** ratio is increased from 1.1 : 1 to 3 : 1, and the H5/H6 cross-peaks of C^5 and C^{11} bases disappear when the Ru : **II** ratio reaches 3 : 1, suggesting that all the G^6 and G^{12} bases are ruthenated in the **I/II** mixture 3 : 1. Assignment: $\text{C}^{1'}$, $\text{C}^1\text{-H}5/\text{H}6$ cross-peak of ruthenated species; $\text{C}^{4'}$, $\text{C}^4\text{-H}5/\text{H}6$ cross-peak of ruthenated species; $\text{C}^{5'}$, $\text{C}^5\text{-H}5/\text{H}6$ cross-peak of ruthenated species. Assignments are based on the 2D [^1H , ^1H] NOESY NMR spectrum (Tables S2–S4†) and HPLC results (Fig. 2); for DNA sequence, see Scheme 1.

towards the coordinated arene ring, see Fig. 1 and Table S5†) of mono-ruthenated duplexes Ru-IIa and Ru-IIb (Ru = $\{(\eta^6\text{-tha})\text{Ru}(\text{en})\}^{2+}$ (**1'**)). No cross-peaks for en-NHu resonances of Ru-IIa and Ru-IIb were detectable after the equilibrium mixture had been freeze-dried and re-dissolved in D₂O at 283 K. The en-NHd resonances of both Ru-IIa and Ru-IIb were not observed in either H₂O or D₂O solutions. In contrast, the en-NHu and en-NHd resonances of unreacted **1** were detected in 90% H₂O (Fig. S3†). The assignments are listed in Table S5.†

2D [¹H, ³¹P] HSQC NMR of 1.1 : 1 I/II reaction

The backbone phosphate ³¹P (−0.6 to −1.4 ppm) to sugar ring H3' (5.3–4.6 ppm) and H4' (4.6–4.0 ppm) HSQC connectivities for free duplex II and the 1.1 : 1 I/II reaction are shown in Fig. 4 and the assignments are listed in Tables S3 and S4.† Compared to free duplex II, the ³¹P/H4' cross-peaks for C⁴ (peak e) and G^{6*} (peak i) residues, ³¹P_{n+1}/H3'_n cross-peaks for G²-G^{3*} (peak d), G^{3*}-C⁴ (peak f) and C⁴-C⁵ (peak h) residues were shifted to give new peaks, but ³¹P/H4' cross-peaks for G^{3*}, C⁴ and C⁵ (peak g) and ³¹P_{n+1}/H3'_n cross-peaks for C⁵-G^{6*} (peak j) residues were too broad to assign. Decreased intensities of ³¹P/H4' and ³¹P_{n+1}/H3'_n cross-peaks were found for G²/G⁸ (peak b), G³/G⁹ (peak c), and

C⁴/C¹⁰ (peak d) residues. These results are consistent with the HPLC-MS and 2D TOCSY NMR data.

2D [¹H, ¹H], [¹⁵N-edited [¹H, ¹H] NOESY NMR of products from 1.1 : 1 I/II reaction

Assignments for ¹H NMR peaks of mono-ruthenated duplexes Ru-IIa and Ru-IIb in the spectra of the 1.1 : 1 I/II reaction are listed in Tables 1, S3 and S4,† and intermolecular NOEs in Tables S6 and S7.† For Ru-IIa, a large low-field shift of the G³H8 resonance was observed, as was also the case for H8 of the neighbouring G² base and H5 and H6 of the neighbouring C⁴ base, relative to free duplex II (Fig. S4 and Tables S2 and S3†). The largest changes in deoxyribose H1' chemical shifts occur for G^{3*}, G² and C⁵ residues, with the smallest changes for the neighbouring C⁴ and C¹⁰ residues (Fig. S4 and Table S3†). NOE cross-peaks were found between G^{3*}H8 and 1'-en-NHd, 1'-en-NHu, H2,3, H1,4 and H9,10 protons, between G^{3*}H1', G^{3*}H2'/H2'' and 1'-H9,10 and H1,4 protons, between C⁴-H5', C⁴-H6 and 1'-H9,10 and H1,4 protons, and between C⁴-H1' and 1'-H9,10, H5,8 protons (Figs. 5, S6 and Table S6†). NOE cross-peaks were also found between protons of bases G⁹, G² and C¹⁰ and 1'. In particular, NOE cross-peaks were observed between G⁹H2'', C¹⁰-H1' and 1'-H6,7 (Figs. 5, S6 and Table S6†). Sequential connectivities for base-to-sugar ¹H NMR resonances were obtained, but those in the G²-C^{3*}, G^{3*}-C⁴ and G⁹-C¹⁰ steps were extremely weak or absent. The interruption or weakening of NOE connectivities between sequential DNA nucleotides is consistent with the binding of $\{(\eta^6\text{-tha})\text{Ru}(\text{en})\}^{2+}$ (**1'**) at G^{3*} in the adduct Ru-IIa.

For adduct Ru-IIb, large low-field shifts were observed for the G^{6*}H8 resonance and for H5 and H6 resonances of the neighbouring C⁵ residue (Fig. S5 and Tables S2 and S4†). The H6 resonance of C⁷ in the complementary strand, which is paired with G⁶, shifted slightly to low field, but the H5 resonance shifted to high-field relative to free duplex II. The largest changes in H1' chemical shifts were found for G⁸, and for C⁷, C⁵, and G^{6*}. NOE cross-peaks were found between G^{6*}H8 and 1'-en-NHd, 1'-en-NHu, H2,3, H1,4, H9,10 and H5,8 protons, between G^{6*}-H1' and 1'-H9,10, H5,8 and H6,7 protons, and between G^{6*}-H4', G^{6*}-H5' and 1'-H9,10 and H5,8 protons (Figs. 5, S6 and Table S7†). NOE cross-peaks were also detected between protons of the bases C⁵, G⁸, C⁷ and bound fragment 1' (Figs. 5, S6 and Table S7†). Particularly of note were cross-peaks observed between C⁷-H2' and 1'-H6,7, C⁷-H2'' and 1'-H5,8. Sequential base-to-sugar connectivities were obtained, but those in the C⁴-C⁵, C⁵-G^{6*} and C⁷-G⁸ steps were extremely weak or absent. The interruption or weakening of NOE connectivities between sequential DNA nucleotides is consistent with the binding of 1' at G^{6*} in the adduct Ru-IIb.

Only one set of signals was observed for the bound fragment $\{(\eta^6\text{-tha})\text{Ru}(\text{en})\}^{2+}$ (**1'**) in the two ruthenated duplexes Ru-IIa and Ru-IIb (Figs. 5, S6† and Table 1). Compared to the unbound chloro form of **1**, peaks for 1'-H1/H4 and H2/H3 of the coordinated arene (see Fig. 1 for labelling) were shifted to low-field, the largest shift being for 1'-H1/H4 (Table 1). Peaks for 1'-H9/H10, H5/H8 and H6/H7 of the non-coordinated rings were shifted to low-field by +1.00, +0.12 and +0.09 ppm, respectively, the largest shift being for 1'-H9/H10 ($\Delta\delta = +1.00$ ppm). Two sets of slightly

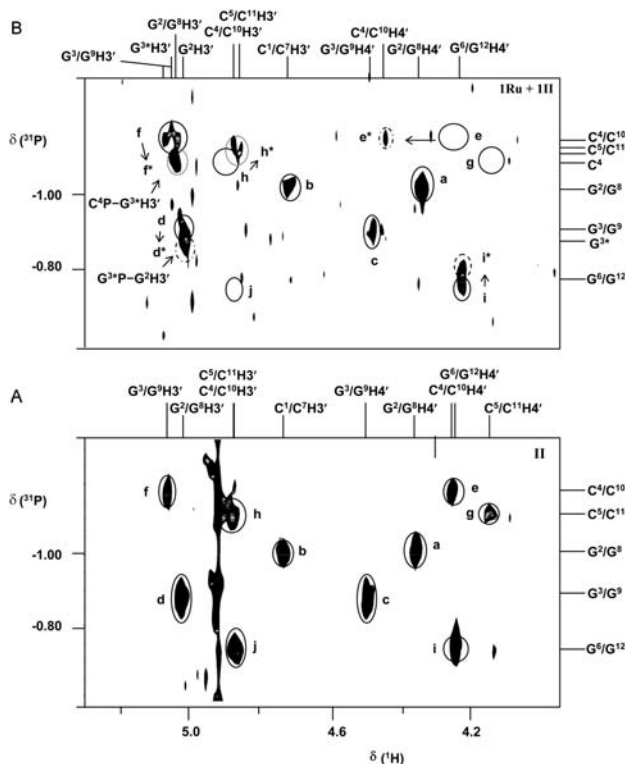


Fig. 4 2D [¹H, ³¹P] HSQC NMR spectra of (A) duplex II and (B) 1.1 : 1 I/II mixture (0.34 mM, 0.1 M NaClO₄ at 283 K, pH 7.0) in 90% H₂O/10% D₂O, showing the backbone ³¹P (−1.4 to −0.60 ppm) to sugar ring H3' (5.2–4.6 ppm) and H4' (4.6–4.0 ppm) connectivities. The circles indicate Cⁿ⁻³¹P/H4', Cⁿ⁻³¹P/Cⁿ⁻¹-H3' and Cⁿ⁻³¹P/Gⁿ⁻¹-H3' or Gⁿ⁻³¹P/H4', Gⁿ⁻³¹P/Gⁿ⁻¹-H3' and Gⁿ⁻³¹P/Cⁿ⁻¹-H3' assignments. Note the disappearance of cross-peaks g and j, downfield shift of cross-peaks d, e, f, h and i to give new peaks d*, e*, f*, h* and i*, respectively, and decrease in intensity of cross-peaks c, d and f after ruthenation of G³N7 (Ru-IIa) and G⁶N7 (Ru-IIb). For DNA sequence, see Scheme 1.

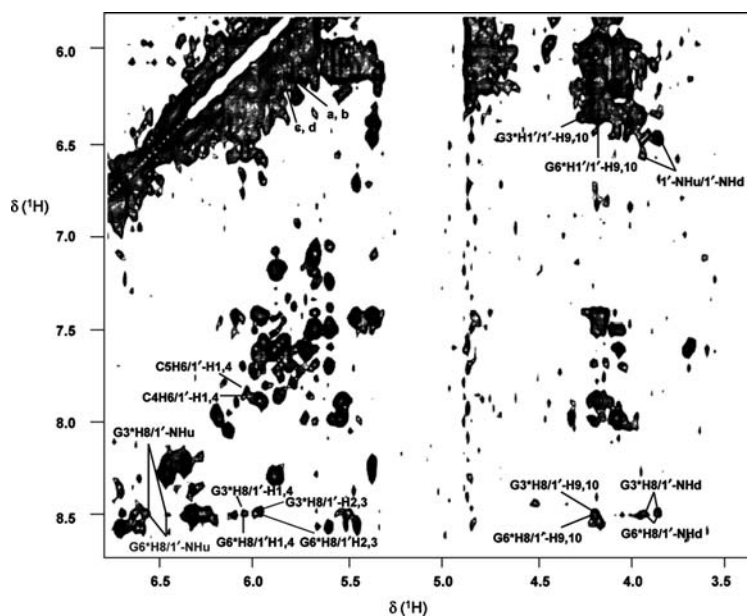


Fig. 5 Part of the 2D [^1H , ^1H] NOESY NMR spectrum of the 1 : 1 equilibrium mixture of duplex **II** and complex **1** (0.34 mM, 0.1 M NaClO_4 , 90% H_2O /10% D_2O at 283 K, pH 7.0, mixing time 400 ms). Cross-peaks: a, $\text{G}^2\text{H}1'/1'-\text{H}6,7$; b, $\text{C}^{10}\text{H}1'/1'-\text{H}6,7$; c, $\text{G}^3\text{H}1'/1'-\text{H}6,7$; d, $\text{C}^7\text{H}1'/1'-\text{H}6,7$. The observed intermolecular $\{(\eta^6\text{-tha})\text{Ru}(\text{en})\}^{2+}\text{-II}$ cross-peaks from mono-ruthenated product **II-Ru-G**³ are: $\text{G}^{3*}\text{H}8/1'-\text{enNHu}$, $\text{G}^{3*}\text{H}8/1'-\text{enNHd}$, $\text{G}^{3*}\text{H}8/1'-\text{H}9/10$, $\text{G}^{3*}\text{H}8/1'-\text{H}1,4$, $\text{G}^{3*}\text{H}1'/1'-\text{H}9/10$, $\text{G}^{3*}\text{H}1'/1'-\text{H}1,4$, $\text{C}^4\text{H}6/1'-\text{H}1,4$, $\text{C}^4\text{H}6/1'-\text{H}9,10$, $\text{C}^4\text{H}5/1'-\text{H}9,10$, $\text{G}^9\text{H}1'/1'-\text{H}6,7$, $\text{C}^{10}\text{H}1'/1'-\text{H}6,7$; and from **II-Ru-G**⁶ are: $\text{G}^{6*}\text{H}8/1'-\text{enNHu}$, $\text{G}^{6*}\text{H}8/1'-\text{enNHd}$, $\text{G}^{6*}\text{H}8/1'-\text{H}9/10$, $\text{G}^{6*}\text{H}8/1'-\text{H}1,4$, $\text{G}^{6*}\text{H}1'/1'-\text{H}9/10$, $\text{C}^5\text{H}6/1'-\text{H}1,4$, $\text{G}^8\text{H}1'/1'-\text{H}6,7$, $\text{C}^7\text{H}1'/1'-\text{H}6,7$. Cross-peaks within the ruthenated guanine residues G^{3*} or G^{6*} , and within the bound ruthenium complex **1** are also indicated. Labels: **1**' = $\{(\eta^6\text{-tha})\text{Ru}(\text{en})\}^{2+}$; ruthenated guanines are marked with asterisks. For NMR chemical shifts, see Tables S2–S4,† and for atom labels, see Fig. 1.

low-field-shifted or unchanged signals for **1**'-en CH_2 of both **Ru-IIa** and **Ru-IIb** were detected. Two sets of signals for both **1**'-en-NHd and en-NHu protons of **Ru-IIa** and **Ru-IIb** were observed, and the peaks for **1**'-NHd and NHu were shifted to low-field, the largest shift being for **1**'-NHu. One set of signals from unreacted ruthenium complex **1** was observed in the 1.1 : 1 **I/II** reaction mixture (Fig. S7† and Table 1). These results are consistent with ROESY experiments (data not shown).

Discussion

Complex **1** selectively ruthenates guanine bases in single strand DNA **I** or duplex **II** (Fig. 2a–c) with a similar pattern to that observed for the biphenyl (bip) and *p*-cymene (cym) complexes.²² Complex **1** is as reactive towards duplex **II** as the Ru-bip complex, and much more reactive than the Ru-cym complex. This pattern of reactivity was observed previously with calf thymus DNA, for which $t_{50\%}$ values of 10 min, 10 min and 3.5 h for complexes **1**, Ru-bip and Ru-cym, respectively, were found.²⁶

Precipitation of adducts was observed when >1 mol equiv. of Ru-bip or Ru-cym complex was added to duplex **II** (0.2 mM).²² However, no such behaviour was observed in the present work. Addition of up to 3 mol equiv. of complex **1** to duplex **II**, even at the higher concentration of 0.3 mM, did not result in precipitation. This suggests that the nature of the arene influences intermolecular interactions. However, precipitation of adducts was observed when >3 mol equiv. of complex **1** was added to duplex **II** (0.3 mM), and was also the case when the reaction mixture of **1** + **II** (3 : 1) was kept at 277 K for long periods (*ca.* four weeks).

Intermolecular interactions are probably also influenced by the order of occupation of the Ru sites and the extent of arene intercalation (for tha and bip).

Determination of binding sites by NMR

The ^{31}P chemical shift changes determined from the 2D [^1H , ^{31}P] HSQC NMR experiment are consistent with ruthenation at N7 of the G residues of the 6-mer DNA duplex **II** by **1**. Binding of Ru-bip to the phosphate of 5'-GMP^{27,28} causes a low-field shift of the ^{31}P NMR resonance by up to +5.11 ppm. However, the binding of Ru-bip to N7 of 5'-GMP,²⁸ 5'-IMP or 5'-cGMP caused low-field ^{31}P NMR shifts of less than 1 ppm. Similarly, ruthenation of 5'-GMP by *trans*- $[\text{RuCl}_2(\text{DMSO})_4]$ giving Ru-OPO₃ coordination causes a +5.8 ppm ^{31}P downfield shift,⁶² and direct Pt-OPO₃ binding to IMP produces a ^{31}P downfield shift of about +3.5 ppm.⁶³ The formation of N7-ruthenated complexes of 5'-GMP and 5'-IMP, N6- or N4-ruthenated complexes of 5'-AMP or 5'-CMP by $\{\text{Ru}(\text{III})(\text{NH}_3)_5\}^{3+}$ gave rise to little change in ^{31}P resonances of the nucleotides.⁶⁴ Therefore, it is evident that direct coordination of Ru^{II} to a phosphate oxygen induces a ^{31}P chemical shift change of *ca.* +5 ppm, while coordination to GN7 and no direct binding to phosphate oxygen induces a chemical shift change in the range of 0–1 ppm. In the present case, the most affected signals are assigned to the phosphate groups of residue C⁴ ($\Delta\delta$ +0.09 ppm) and residue G^{6*} ($\Delta\delta$ –0.05 ppm) (Fig. 4 and Tables S3 and S4).† Other ^{31}P resonances are shifted by less than 0.03 ppm. Significant changes were observed for ^{31}P , H3' and H4' resonances of residues G^{3*}, C⁴, C⁵ and G^{6*}; minor

changes observed for the corresponding resonances of C¹/C⁷ and G²/G⁸ further indicated that the binding site was N7 of G^{3*} or G^{6*}. Selective binding to N7 of the G residues of double-stranded DNA duplex **II** was evident from the ¹⁵N-edited [¹H, ¹H] NOESY NMR spectrum and confirmed by ¹H NMR chemical shift changes (Figs. 5, S6 and Tables S3 and S5†). NOE connectivities between ruthenated G^{*}H8 and I'-NHu or I'-NHd were observed in the ¹⁵N-edited [¹H, ¹H] NOESY and ¹⁵N-decoupled [¹H, ¹H] NOESY NMR spectra. Binding of **I** to 9-ethylguanine and 5'-GMP²⁷ via N7 causes a low-field shift of the H8 ¹H NMR resonance by up to +0.6 ppm. Binding of Ru-cym and Ru-bip complexes to 6-mer single strand DNA **I** or duplex **II**²³ via N7 causes low-field shifts of the H8 ¹H NMR resonance of +0.49 to +0.66 ppm, and +0.28 to +0.58 ppm, respectively. Similar shifts were observed for the H8 resonances of G bases in the hexamer, and allow assignment of the binding sites as G^{3*} ($\Delta\delta$ H8 + 0.59 ppm) in Ru-**IIa** and G^{6*} ($\Delta\delta$ H8 + 0.46 ppm) in Ru-**IIb** present in the 1:1:1 reaction mixture of **I** + **II** (Figs. S1, S4 and S5, Tables S3 and S4†). With the binding fragment $\{(\eta^6\text{-tha})\text{-Ru}(\text{en})\}^{2+}$ (**I'**), the mono-ruthenated duplex Ru-**IIa** is assigned as **II-Ru-G³(I')**, Ru-**IIb** as **II-Ru-G⁶(I')** (for DNA sequence, see Scheme 1).

The ruthenation of duplex **II** by complex **I** mainly caused low-field shifts of imino proton resonances of G residues G^{3*} and G⁹ in **II-Ru-G³(I')**, but high field shifts of imino proton resonances of G residues G^{6*} and G¹² in **II-Ru-G⁶(I')** (Fig. S2 and Tables S3 and S4†). In contrast, the imino proton resonances of the mono-intercalated duplexes and di-intercalated duplex ruthenated with Ru-bip are broad and weak, implying that the base-pairs are disrupted in the duplex with an increase in dynamic mobility of the bases.²³ High-field shifts of imino proton resonances were found for mono-ruthenated species in the 1:1 reaction mixture of Ru-cym complex + **II**, and platination of the 14-mer duplex d(TATGTACCATGTAT)/d(ATACATGGTACATA) also causes high field shifts of G imino proton resonances.^{23,59}

Structural perturbations induced by ruthenation with complex **I** are larger than those observed for Ru-bip and Ru-cym complexes,²³ and are localized to within a few (± 2) base-pairs of the ruthenation site in all cases for complex **I**, while only the two adjacent bases (C⁴ and C¹⁰ or C⁵ and C⁷) are affected by ruthenation at G^{3*} or G^{6*} in all cases for Ru-bip and Ru-cym adducts. Not only were large low-field shifts of the H5 and H6 resonances observed for C⁴ in **II-Ru-G³(I')** and C⁵ in **II-Ru-G⁶(I')**, but also for H1' of G², G³, C⁴, C⁵ and C¹¹ in **II-Ru-G³(I')**, and of C⁵, C⁷ and G⁸ in **II-Ru-G⁶(I')** (Tables S3 and S4†).

Intercalation

Literature reports show that intercalation into DNA base pairs can often be recognised by distinctive features,^{19,22,23,49,54,61,65} including (a) upfield ¹H NMR shifts of resonances of the intercalator; (b) NOE cross-peaks between protons of the intercalator and DNA bases at sites of intercalation; (c) the interruption or weakening of NOE connectivities between sequential DNA nucleotides; (d) the absence or weakening of the correlation peaks of H3'_n-³¹P_{n+1} and H3'_n-³¹P_n at sites of intercalation steps and the large chemical shift perturbations at the intercalation steps; and (e) the weakening of the strength of H-bonding between en-NH and GO6 in the case when the ruthenium

complex Ru-bip with an extended arene ring system was involved.^{22,23}

It is notable that no large high-field shifts of proton resonances of **I'** were detected, but large low-field shifts up to +1.00 ppm were observed for protons H9,10, H5,8 and H6,7 of rings B and C in the mono-ruthenated duplexes **II-Ru-G³(I')** and **II-Ru-G⁶(I')** (Table 1). These shifts are inconsistent with shielding effects from the ring-currents of nucleobases which form a sandwich with the intercalated non-coordinated rings of bound **I'**, and so do not provide evidence for intercalative binding.^{19,49,54,65} For example, upfield shifts of between -0.4 and -1.0 ppm have been reported for Ru-bip intercalated into 6-mer or 14-mer duplex DNA,^{22,23} and upfield shifts of -0.1 to -1.0 ppm for the intercalated dap (1,12-diazaperylene) ligand of the dirhodium(II) carboxylate complex [Rh₂(dap)(CH₃COO)₃(CH₃OH)₃] into a 12-mer duplex DNA.¹⁹ Such large low-field shifts of the bulky tha intercalator have not been observed for other bulky intercalators, for example, large high-field shifts have been observed for bulky intercalated cholesterol groups.⁴⁴ However, similar large low-field shifts for proton resonances of I'-9EtG were found for the adduct $[(\eta^6\text{-tha})\text{Ru}(\text{en})(9\text{EtG})]$,²⁸ the H5,8 and H6,7 resonances slightly shifted to high-field, but the H9,10 resonances remained unchanged. In the case of $[(\eta^6\text{-tha})\text{Ru}(\text{en})(5'\text{-GMP})]$ (**I'-GMP**),²⁸ H9,10 and H5,8 resonances are shifted to low-field by +0.83 and +0.50 ppm, respectively, and the H6,7 resonances shifted to high-field by -0.10 ppm. In the present case of the mono-ruthenated duplexes **II-Ru-G³(I')** and **II-Ru-G⁶(I')**, H9,10, H5,8 and H6,7 resonances shifted to low-field by +1.00, +0.12 and +0.09 ppm, respectively. Thus it is reasonable that the resonances of intercalated non-aromatic rings B and C of tha in the mono-ruthenated duplexes **II-Ru-G³(I')** and **II-Ru-G⁶(I')** shift to low field.

The single crystal X-ray structure of (**I'-GMP**)²⁸ shows that ring C of **I'** is tilted towards the purine by 27.8° and lies directly over the purine base, indicative of strong intramolecular π - π stacking separation of 3.45 Å and dihedral angle of 3.3°. Intercalation of the non-coordinated rings of **I'** into the DNA duplex is also consistent with circular and linear dichroism data.^{26,29} Due to excessive resonance broadening, the resonances for protons that intercalate between purine rings are difficult to assign. Weak to intermediate intensity NOE cross-peaks were found not only between the rings of bound **I'** and H1' or H8 protons of G^{3*} or C⁴ in **II-Ru-G³(I')**, but also between the rings of **I'** and G⁹ and C¹⁰ (Figs. 5, S6 and Table S6†). This can happen if the intercalation occurs not only at the G³pC⁴ base step, but also at the G⁹pC¹⁰ base step. The intermediate intensity cross-peaks observed between G⁹H2'' or C¹⁰H1' and I'-H6,7 protons, indicate that the extended rings of **I'** intercalate deeply and are located between the middle of G⁹ and C¹⁰ bases. Analogous NOE cross-peaks between the rings of bound **I'** and H1', H8, H2' and H2'' of G^{6*} in **II-Ru-G⁶(I')**, and also between rings of **I'** and C⁵, C⁷ and G⁸ were detected, indicating that intercalation occurs between G^{6*} and C⁵, and between G⁸ and C⁷ as well (Figs. 5 and S6, and Table S7†). The intermediate intensity cross-peaks observed between G⁶ or C⁵ and I'-H1,4 protons, indicate that the coordinated arene ring of **I'** is located between the middle of G⁶ and C⁵ bases. Additionally, intermediate intensity cross-peaks observed between C⁷H2' and I'-H6,7 and C⁷H2'' and I'-H5,8 protons indicate that the extended rings of

1' intercalate deeply and are located near to the **C**⁷ base. The interruption of NOE connectivity pathways between the corresponding base pairs (**G**²-**C**^{3*}, **G**^{3*}-**C**⁴ and **G**⁹-**C**¹⁰ steps in **II**-Ru-**G**³(**1'**), and **C**⁴-**C**⁵, **C**⁵-**G**^{6*} and **C**⁷-**G**⁸ steps **II**-Ru-**G**⁶(**1'**)) is consistent with these intercalation sites.

The absence of the **H**_{3'_n-P_{n+1} cross-peaks linking the **C**⁵-**G**^{6*} step and the **H**_{3'-P} cross-peaks of **G**^{3*}, **C**⁴ and **C**⁵, the low field shifts for **H**_{3'_n-P_{n+1} cross-peaks linking **G**²-**G**^{3*}, **C**⁴-**C**⁵ and **G**^{3*}-**C**⁴, and for **H**_{3'-P} cross-peaks of **C**⁴/**C**¹⁰ and **G**⁶, and the large chemical shift perturbations at the **G**²-**G**^{3*} and **C**⁵-**G**^{6*} steps, together indicate that the intercalation occurs between **G**³p**C**⁴ or **C**⁵p**G**⁶ base steps (Fig. 4).⁶² Previous work has shown that the intercalation sites of the non-coordinated phenyl ring of Ru-bip in mono-ruthenated duplexes^{4c} are also between **G**³p**C**⁴ or **C**⁵p**G**⁶ base steps.}}

No cross-peaks for en-NHu resonances of Ru-**IIa** and Ru-**IIb** were detected after the 1.1 : 1 **I/II** reaction mixture had been freeze-dried and re-dissolved in D₂O. This suggests that the hydrogen bond between **G**^{*}O6 and en-NH of **1'** is weakened (Fig. S3 and Table S5†), which is consistent with intercalation of the non-coordinated rings of **1'** into duplex DNA **II**. Similarly weakened hydrogen bonds were also observed when the biphenyl ring of Ru-bip intercalates into the hexamer duplex.²² The strength of the H-bond between **G**^{*}O6 and en-NH is related to the decay rate of the en-NH signals when **II**-Ru adducts are dissolved in 99% D₂O.²² For the non-intercalated adduct with Ru-cym, the half-life was 72 h. However, those of the mono- and di-intercalated Ru-bip adducts were only 5 h and <0.1 h, respectively.

NMR studies show that the arene–nucleobase π–π stacking of **1'** with hexamer duplex is different from that of Ru-bip.^{22,23} Only a very few weak NOE contacts between protons of ring B of biphenyl and **H**_{1'} and **H**_{2'/H}_{2''} protons of **G**^{3*} or **C**⁴ of the hexamer duplex are observed.²² The protons **H**_{o'}, **H**_{p'} and **H**_{m'} of bound Ru-bip in the DNA duplex adducts were consistently shielded relative to free Ru-bip, consistent with base stacking of the non-coordinated ring B between base pair **G**^{3*}p**C**⁴. However, in the present case, not only were weak to intermediate intensity NOE contacts detected between protons of rings B and C of tha and protons of **G**^{3*} and **C**⁴ or **G**^{6*} and **C**⁵, but also intermediate intensity NOE contacts were detected between protons of ring C of tha and protons of **G**⁹ and **C**¹⁰ or **C**⁷ and **G**⁸ DNA bases which pair with **G**^{3*} or **C**⁴, **G**^{6*} or **C**⁵ in the complementary DNA strand (Fig. 5, Tables S6 and S7†), respectively. This indicates that rings B and C of tha are involved in a penetrative intercalation between two pairs of bases, **G**³/**C**¹⁰:**C**⁴/**G**⁹ or **G**⁶/**C**⁷:**C**⁵/**G**⁸. It is interesting that large low-field shifts, but not large high-field shifts are observed for the proton resonances of intercalated rings B and C of **1'**, indicating that the intercalative interactions between Ru-tha and Ru-bip with the DNA duplex are significantly different from one another. The ring current shifts are position-related: upfield shifts only arise when the protons are above or below the ring plane. In contrast, resonances for protons located close to the plane and beyond the confines of the ring are shifted to low field.⁶⁶

Modelling of **II**-Ru-**G**³(**1'**) and **II**-Ru-**G**⁶(**1'**)

In order to attempt to rationalize the NOE and chemical shift information gathered for **II**-Ru-**G**³(**1'**) and **II**-Ru-**G**⁶(**1'**), two

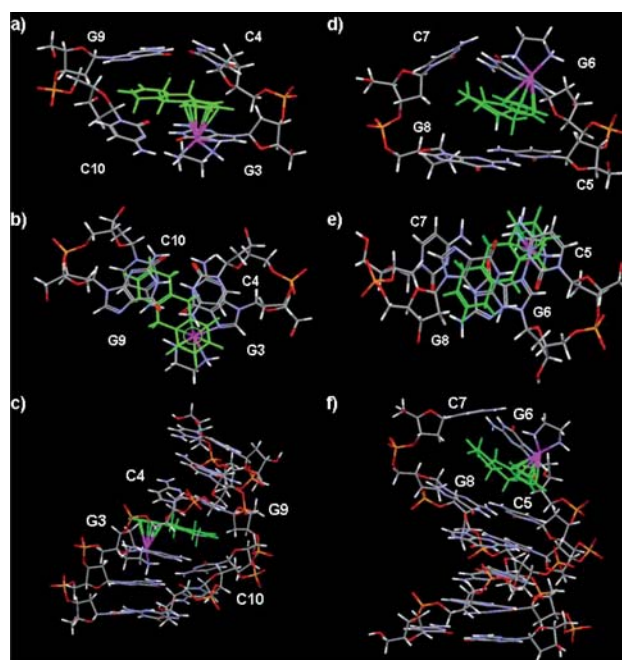


Fig. 6 Molecular models of duplex **II** ruthenated at N7 of **G**³ or N7 of **G**⁶ with $\{(\eta^6\text{-tha})\text{Ru}(\text{en})\}_2^{2+}$. (a)–(c) **II**-Ru-**G**³ showing the intercalation of the tetrahydroanthracene ligand between **G**³/**C**¹⁰:**C**⁴/**G**⁹. (d)–(f) **II**-Ru-**G**⁶ in which the non-arene rings are intercalated between **G**⁶/**C**⁷:**C**⁵/**G**⁸. In each case side and top views of the intercalation site are shown as well as the whole duplex (bottom). Colour code: tha green, Ru purple, P yellow, O red.

molecular models were constructed in which the duplex d(CGGCCG)₂ was ruthenated at N7 of **G**³ or **G**⁶ by **1'**, as shown in Fig. 6. The **II**-Ru-**G**³(**1'**) (Fig. 6a–c) and **II**-Ru-**G**⁶(**1'**) (Fig. 6d–f) models are mostly consistent with the NMR observations, and overwhelming evidence indicates that a penetrative interaction occurs between rings B and C of **1'** and duplex DNA at **G**³/**C**¹⁰:**C**⁴/**G**⁹ or **G**⁶/**C**⁷:**C**⁵/**G**⁸, respectively. The model also provides a useful indication of how **1'** may lie in relation to its DNA binding site. The **H**_{5,8} and **H**_{9,10} protons of **1'** are located above or below the ring plane and the distances between **H**_{5,8} or **H**_{9,10} protons and purine or pyrimidine rings of **G** or **C** bases are nearly 0.9 Å shorter than the case of aromatic intercalators, such as Ru-bip. Compared to the structural findings for aromatic intercalators, both structures (**II**-Ru-**G**³(**1'**) and **II**-Ru-**G**⁶(**1'**)) suggest distortion of bases-pair planes around the site at which the tha has penetrated and the system is likely to be highly dynamic in and around the intercalation sites. The dynamics of **II**-Ru-**G**⁶(**1'**), in which the Ru binds to a terminal, potentially frayed nucleotide, would be expected to be significantly different compared with those for **II**-Ru-**G**³(**1'**), in which the Ru binds to the internal base.

The data imply that in both cases the tha of **1'** in the models has swung round so that the ring system points across to the opposite strand rather than penetrating so deeply into the strand to which the Ru centre is attached (**G**^{3*} or **G**^{6*}). This supports the NOE contacts observed between protons of rings A and B of **1'** and **H**_{1'} and **H**₈ or **H**₆ protons of **G**³, **C**⁴ or **C**⁵, **G**⁶ and in particular between **H**_{6,7} protons of ring C of **1'** and the **H**_{1'}, and **H**_{2'} protons of residue **C**¹⁰, **G**⁹ or **G**⁸, **C**⁷ of the complementary

strand (see Tables S6 and S7,† Fig. 6). In contrast in models for Ru-bip, the non-coordinated phenyl ring of the biphenyl ligand penetrates deeply at the G^{3*}pC⁴ or G^{6*}pC⁵ base step. The relevant inter-proton distances are consistent with the observed NOE contacts. Observed NOE data are consistent with the model of **II**-Ru-G³(**I'**): NOEs occur between H1,4 (~3.45 Å), H9,10 (~4.73 Å), H2,3 (~3.72 Å) and G^{3*}H8, respectively; between H9,10 (~4.74 Å) or H1,4 (~4.64 Å) and G^{3*}H1', respectively; between H9,10 (~3.71 Å) or H1,4 (~3.24 Å) and C⁴H6, H5,8 (~3.60 Å) or H9,10 (~4.14 Å) and C⁴H1', respectively; between H6,7 (~3.67, 3.18 or 2.52 Å) and G³H1', -H2' or -H2'', respectively; between H6,7 (~2.94 or 2.69 Å), H5,8 (~3.08 Å) and C¹⁰H6 or C¹⁰H1', respectively and NHd (~2.49 or 3.03 Å) and G²H8 or -H2' in the model, respectively. Observed NOE data are also consistent with the model **II**-Ru-G⁶(**I'**): medium and weak NOEs occur between H1,4 (~2.74 Å) or H9,10 (~2.86 Å) and G^{6*}H8, respectively; between H5,8 (~2.55 Å), H9,10 (~3.47 Å) and G^{6*}H1', respectively; between H1,4 (~2.87 Å) and C⁵H6, H1,4 (~3.72 Å) and C⁵H1', H1,4 (~2.66 Å) and C⁵H2', respectively; between H6,7 (~2.44 Å) and C⁷H2', H6,7 (~2.94 Å) and C⁷H1', H6,7 (~3.01 Å), H5,8 (~2.53 Å) and C⁷H2'', H6,7 (~3.44 Å), H5,8 (~3.50 Å) and G⁸H1', H5,8 (~3.85 Å), H6,7 (~3.89 Å) and G⁸H2'/H2'' in the model, respectively. As shown in Fig. 6, the shortest distance for enNH...O6G³ or enNH...O6G⁶ is 2.66 or 2.01 Å, larger than that in the reported 9EtG adduct (1.91 Å),²⁸ consistent with weak en-NH resonances observed for **II**-Ru-G³(**I'**) and **II**-Ru-G⁶(**I'**) in D₂O.

The largest downfield shift (+1.00 ppm) is observed for H9,10 protons of ring B of **I'** for mono-ruthenated duplexes **II**-Ru-G³(**I'**) and **II**-Ru-G⁶(**I'**) (Table 1), but the shift changes for H6,7 (+0.09 ppm) and H5,8 (+0.12 ppm) of ring C of **I'** are rather small when compared with that for H9,10. These results are consistent with the base stacking of the non-coordinated rings and formation of short C-H...X (X = O or N)⁶⁷ hydrogen bonds between the protons of non-coordinated rings and bases as shown in models **II**-Ru-G³(**I'**) and **II**-Ru-G⁶(**I'**) (Fig. 6). It is clear that H5,8 and H6,7 protons are located within the confines of the purine ring G⁹ in model **II**-Ru-G³(**I'**) or G⁶ in **II**-Ru-G⁶(**I'**), and the H9,10 protons are located exactly in the middle of the two strands (Fig. 6) and in the ring planes beyond the confines of the purine or pyrimidine rings.

It has been reported that proton chemical shifts may change by up to +2.1 ppm (downfield) on formation of C-H...X (X = O or N) hydrogen bonds.⁶⁸ It is clear in the present case that the protons of rings B and C do sit near the edge of the purine or pyrimidine rings from the models **II**-Ru-G³(**I'**) and **II**-Ru-G⁶(**I'**), and the protons are not directed to the centres of these rings. Other than the fact that protons of ring B are within the arene ring plane in Ru-bip, the H5,8 and H9,10 protons of **I'** are located above or below the ring plane in the models. Such orientation makes the distances between H5,8 or H9,10 and N or O atoms of purine or pyrimidine rings of G or C bases nearly 0.9 Å shorter than those of Ru-bip. For model **II**-Ru-G³(**I'**): short H9,10...N1 of G³ (~2.68 Å), H9,10...N3 of C⁴ (~2.51 Å), H5,8...N1 or N7 of G⁹ (~2.70 or 2.75 Å, respectively), H5,8...OC2 of C⁴ (~2.60 Å), H6,7...sugar O of G⁹ (~2.58 or 2.80 Å, respectively) distances are observed (Fig. 6a–c). For model **II**-Ru-G⁶(**I'**): short H9,10...N9 of G⁶ (~2.66 Å), H9,10...N3 of C⁵ (~2.54 Å), H5,8...N3 of G⁶, C⁷ and G⁸ (~2.60, 2.61 or 2.61 Å,

respectively), H6,7...OC2 of C⁷ (~2.59 Å) distances are observed (Fig. 6d–f). Thus, in the present case, the shifts of the protons of rings B and C of **I'** reflect both the downfield shift induced by the formation of C-H...X (X = O or N) hydrogen bonding,⁶⁸ and the upfield shift induced by the intercalation effect on the protons located above or below the intercalator, due to the ring current effect of the aromatic groups. The H9,10 protons are located exactly central to the two strands of DNA, so the downfield shifts for H9,10 protons are larger (1.0 ppm).

The data imply that in both cases the tha of **I'** in the models has swung round so that the ring system points across to the opposite strand rather than penetrating so deeply into the strand to which the Ru centre is attached (G^{3*} or G^{6*}). This tendency is then likely to be stabilized by tha–base interactions and C-H...X (X = O or N) hydrogen bonding within the G³-tha ring-C⁴ and the G⁹-tha ring-C¹⁰ 'sandwich' as shown in Fig. 6a–c, or within the G⁶-tha ring-C⁵ and the G⁸-tha ring-C⁷ 'sandwich' as shown in Fig. 6d–f. This kind of intercalation distorts the DNA more than that of aromatic intercalators, such as Ru-bip, and reduces the strength of H-bonding between en-NH and G³O6. The intercalation of the non-coordinated phenyl ring of Ru-bip,²² of actinomycin D (ActD) and daunomycin⁶⁵ between the GC step in previous work suggested that steric crowding at the GpC step is less than that at the GpG step, which thereby allows accommodation of the bulky non-aromatic rings of tha. A further driving force for GpC rather than GpG intercalation is the weaker purine–pyrimidine π–π stacking interaction for GpC compared with purine–purine GpG steps.⁶⁵ It is interesting in the present work that all of the intercalation of Ru-bound tetrahydroanthracene occurs between GpC base steps, and there is no evidence for intercalation at the GpG base steps.

Ru-en-NH...GO6 H-bonding

Two distinct NHu-NHd cross-peaks were identifiable in the 283 K 2D NOESY and 2D ¹⁵N-edited NOESY NMR spectra (Table S5 and Figs. 5, S6†), and the downfield shifts of NH resonances in the adducts are consistent with the presence of H-bonding to the C6 carbonyl of the coordinated G.^{22,23,27,28} Only one broad peak for NH(u) was detected in the 2D [¹H, ¹⁵N] HSQC NMR data at 283 K; the resonance for NH(d) was too broad to observe (Fig. S3†). NH exchange was rapid for the en-NH(u) protons in the mono-intercalated duplexes **II**-Ru-G³(**I'**) and **II**-Ru-G⁶(**I'**) (no ¹H/¹⁵N cross-peaks being detected for a D₂O solution of **II**-Ru-G³(**I'**) and **II**-Ru-G⁶(**I'**), Fig. S3†). Such a rapid NH exchange of the en-NH(u) protons was also observed in the double-intercalated duplex **II**-Ru₂-G³G⁹(Ru-bip),²² suggesting that mono-intercalation of **I'** into duplex **II** gives rise to similar effects to that of the di-intercalation of Ru-bip.

Sequence specificity of G metallation

Adducts of duplex **II** eluted as single strands from the reverse-phase HPLC column^{22,23} (Fig. 2d and 2e) due to the denaturing character of the HPLC solvent. Three mono-ruthenated products (**I**-Ru-G², **I**-Ru-G³ and **I**-Ru-G⁶) and three di-ruthenated products (**I**-Ru₂-G²G³, **I**-Ru₂-G²G⁶ and **I**-Ru₂-G³G⁶) were detected in the 1 : 1 **I**/**I** reaction mixture, showing that all three guanine bases can be ruthenated readily in the single-stranded

hexamer DNA d(CGGCCG) (Table S1†). Only the two mono-ruthenated products **II**-Ru-G³ and **II**-Ru-G⁶ were detected in the reaction of duplex **II** with **1** at a Ru : **II** molar ratio of 1 : 1; no G² ruthenated adduct was detected (Table S1†). When the above mono-ruthenated products **II**-Ru-G³ and **II**-Ru-G⁶ were reacted with a second mol equiv. of **1** at the same temperature, only two mono-ruthenated single strand adducts (**I**-Ru-G³ and **I**-Ru-G⁶) and two di-ruthenated single strand adducts (likely to be **I**-Ru₂-G³G⁶ and **I**-Ru₂-G²G⁶) eluted from the reverse-phase HPLC column (Table S1†). The products may therefore involve ruthenation on the same strand: **II**-Ru₂-G³G⁶ and **II**-Ru₂-G²G⁶, or on different strands: **II**-Ru₂-G³G⁹, **II**-Ru₂-G⁶G⁹, **II**-Ru₂-G⁶G¹² and **II**-Ru₂-G³G¹². No G⁸ ruthenated duplex adducts such as **II**-Ru₂-G³G⁸ or **II**-Ru₂-G⁶G⁸ were detected. These results are consistent with 2D TOCSY experiments (Fig. 3): the cross-peak intensities of C-H5/H6 (C^{1'}, C^{4'} and C^{5'}) of ruthenated species increased in the 2 : 1 **I/II** reaction mixture.

The cross-peaks for H5/H6 resonances of C⁵/C¹¹ almost disappeared when the Ru : **II** ratio was raised to 3 : 1 (Fig. 3D). This might suggest that the third ruthenation site for the di-ruthenated duplexes occurs at the un-ruthenated G⁶ and G¹² residues, to form two tri-ruthenated duplex adducts: **II**-Ru₃-G³G⁶G¹² and **II**-Ru₃-G²G⁶G¹². Thus, ruthenation of mono-ruthenated products **II**-Ru-G³ and **II**-Ru-G⁶ might result in three di-ruthenated duplex species: **II**-Ru₂-G³G⁶, **II**-Ru₂-G²G⁶ and **II**-Ru₂-G⁶G⁹ (Scheme 1, Table S1†). The HPLC, MS and 2D ¹⁵N-decoupled [¹H, ¹H] TOCSY NMR data indicate that the selectivity of G base ruthenation for the free duplex **II**, mono-ruthenated duplexes and di-ruthenated duplexes is quite different. For free duplex **II**, little ruthenation of G² was observed; for mono-ruthenated duplexes **II**-Ru-G³ and **II**-Ru-G⁶, little ruthenation of G⁸ was observed; however, the favoured ruthenation site for the di-ruthenated duplexes appears to be G⁶ and G¹², the G bases at the 3' end. Reactions of complexes Ru-cym and Ru-bip with duplex **II** d(CGGCCG)₂ at a Ru : **II** ratio of 1 : 1, also gave rise to little ruthenation of G².²² However, the **II**-Ru-G³ : **II**-Ru-G⁶ ratios in the reaction mixtures with Ru : **II** ratio of 1 : 1 are different: 1 : 1 for Ru-cym, 3 : 1 for Ru-bip and 2 : 1 for Ru-tha in the present case, indicating that there is no preference for binding to an internal base or terminal nucleotide for the non-intercalator Ru-cym. In contrast, obvious specificity exists for binding to an internal base for the aromatic intercalator Ru-bip. Specificity for internal bases is also the case for the non-aromatic intercalator Ru-tha. Exclusive attack on the 3'-G (G³), as seen for these organometallic Ru arene complexes, is uncommon for platinum. There might be two reasons for this. Firstly, the pseudo-octahedral coordination site on an arene Ru^{II} complex is more sterically demanding than that of a square-planar site on Pt^{II}. In addition, the steric hindrance around each base in DNA sequences is quite different. The combined steric hindrance of G and C plus the Ru^{II} complex are likely to account for a preferential binding to G³N7 or G⁶N7 rather than to G²N7 in the free duplex. After ruthenation at G³ or G⁶, the situation for the non-ruthenated single strand in the mono-ruthenated products **II**-Ru-G³ and **II**-Ru-G⁶ may be similar to that of the free duplex, so no G⁸ ruthenation is detected. For the mono-ruthenated single strand **I**-Ru-G³ or **I**-Ru-G⁶ in the mono-ruthenated products **II**-Ru-G³ and **II**-Ru-G⁶, steric hindrance around G² in the mono-ruthenated duplex **II**-Ru-G³ is much

greater than that in the free duplex and for this reason it is believed that no **II**-Ru₂-G²G³ species is detected. The DNA distortion caused by ruthenation at N7 of G⁶ may decrease the steric hindrance around G² in the mono-ruthenated duplex **II**-Ru-G⁶, resulting in formation of the G²-bound di-ruthenated duplex **II**-Ru₂-G²G⁶. Steric hindrance around G² and G³ in the di-ruthenated duplexes **II**-Ru₂-G³G⁶, **II**-Ru₂-G²G⁶ and **II**-Ru₂-G⁶G⁹ is even greater, so ruthenation at the end base G⁶ or G¹² as the third site is reasonable.

Bulky lesion and penetrative intercalation

Reported data⁴⁴ show that the intercalative binding of a bulky intercalator cholesterol group on a modified base of a duplex DNA is a classical intercalation, and the lesion site and the distortions in the structure of the DNA produced by these cholesterol derivatives are somehow similar to those induced by other adducts containing polycyclic aromatic groups. However, the base opposite the modified nucleotide is displaced and the local structure of the double helix is highly distorted. These observations are quite different from those in the present work involving penetrative intercalation of tha into duplex DNA when Ru-tha is coordinated at GN7. It is notable that there is no displacement of the base opposite the modified nucleotide, but C-H...X (X = O or N) hydrogen bonding between protons of ring C of tha and O or N atoms of bases opposite the ruthenated nucleotides. The local structure of the ruthenated double helix is highly distorted. Such a highly distorted double helix is not observed in the DNA adducts of platinum complexes with an acridine side arm intercalator, *e.g.* PT-ACRAMTU,⁵⁶ where the threading intercalation occurs at the central base-pair step but does not cause helical bending.

Experimental section

Materials

Organometallic ruthenium(II) complex [(η⁶-tha)Ru(en)Cl][PF₆]₂ (**IPF₆**) (tha = 1,4,9,10-tetrahydroanthracene, en = ethylenediamine) and ¹⁵N-labeled **1** (¹⁵N-**1**) were synthesised as described previously.^{27,28} The sodium salt of FPLC-purified oligonucleotide d(CGGCCG) **I** was purchased from Oswel (Southampton, UK) and was further purified by HPLC. Sodium perchlorate and acetonitrile (HPLC grade) were obtained from Fisher, and triethylammonium acetate buffer (TEAA) from Fluka.

High performance liquid chromatography (HPLC)

This was carried out on reversed-phase columns with TEAA and TEAA/acetonitrile as mobile phases.

HPLC-electrospray ionisation mass spectrometry (HPLC-ESIMS)

Negative-ion electrospray ionisation mass spectra were obtained on a mass spectrometer interfaced with a reversed phase HPLC column eluted with TEAA/acetonitrile gradients as above.

NMR spectroscopy

NMR data were acquired on an 800 MHz or 600 MHz Bruker Avance NMR spectrometer equipped with a multiple resonance TXI (^1H , ^{13}C , ^{15}N , ^{31}P) *xyz*-gradient probe.

Molecular modelling

A structure for canonical B-form duplex $d(\text{CGGCCG})_2$ was generated within the biopolymer module of Sybyl (version 6.3, Tripos Inc.). Crystal coordinates from the X-ray crystal structures of **1** allowed accurate representation of the Ru complex to be incorporated into the model Ru-DNA constructs. Docking of the Ru-complex onto $\text{G}^x\text{N7}$ ($x = 3$ or 6) of the DNA structure was achieved by manual independent manipulation of both DNA and Ru-complex molecules. The Ru-N7 inter-atomic distance was based on reported crystal structures of Ru-GMP complexes. A pseudo-atom at the centre of the η^6 -six-membered aromatic ring (ring A) of tha was attached to the Ru centre to provide a rotatable bond about which the tha moiety could be manipulated. In a similar way, the Ru-GN7 bond was activated to form a rotatable bond, about which the entire Ru ligand could be rotated independently of the DNA structure. Ru- $\text{G}^x\text{N7}$ models were prepared in such a way as to reduce steric contact as far as possible. Constraints were applied where deemed plausible and structures were energy minimized to remove the effects of steric clash.

Details of reactions of **II** with ^{15}N -**I**, HPLC, HPLC-ESI-MS, NMR and pH measurements are in the ESI.†

Conclusions

In conclusion, the results presented here provide a rare example of coordinative binding and the penetrative intercalation of a bulky intercalator into DNA, and may help to explain why ruthenium arene complexes have a different mechanism of antitumour activity (perhaps related to recognition by nucleotide repair enzymes) compared to cisplatin. Firstly, the NMR results were indicative of the penetrative intercalation of the tha rings B and C of **1'**, selectively between two base pairs $\text{G}^3/\text{C}^{10}:\text{C}^4/\text{G}^9$ or $\text{G}^6/\text{C}^7:\text{C}^5/\text{G}^8$, which contrasts with that observed between one base pair G^3/C^4 and or G^6/C^5 for the classic aromatic intercalator Ru-bip. The two slightly different intercalation models for the extended non-aromatic rings of Ru-tha, indicate that the distortion of the DNA duplex is sequence-related. Secondly, large low-field shifts for proton resonances of the intercalated non-coordinated rings B and C of tha reflect both the downfield shift induced by the formation of short $\text{C}-\text{H}\cdots\text{X}$ ($\text{X} = \text{O}$ or N) hydrogen bonds and upfield shift induced by the intercalation effect on the protons located above or below the intercalator, due to the ring currents of aromatic groups. The downfield shifts of H_{9,10} protons of **1'** are larger (+1.0 ppm) for they are located exactly in the middle of the two strands. Such deshielding of intercalator NMR resonances is rare, indicating that the intercalative interactions between this bulky tha intercalator and classical aromatic DNA intercalators are somewhat different. Thirdly, the DNA structural perturbations induced by Ru-tha are larger than those observed for Ru-bip and Ru-cym complexes; distortions of base-pair planes are observed around the sites at which the tha has penetrated, and the dynamics of the

terminal base ruthenated adduct **II-Ru-G⁶(1')** are significantly different from those of internal base ruthenated adduct **II-Ru-G³(1')**. These findings agree with the fact that the precipitation of DNA duplex adducts of Ru-tha is observed only at very high concentrations compared with Ru-bip, suggesting that the intercalation of sterically bulky tha into a DNA duplex makes the duplex DNA behave differently from intercalation by the aromatic bip. Fourthly, selective ruthenation at N7 of G^3 and G^6 in the hexamer DNA duplex is similar to that of Ru-cym and Ru-bip, but the mono-intercalation of tha reduced the strength of H-bonding between en-NH and GO6 as much as that for the di-intercalated di-ruthenated Ru-bip duplex. Intercalation at GpC by tha appears to have a lower energy penalty when compared with intercalation at GpG base steps, thereby allowing accommodation of the non-aromatic, bulky rings of tha. Although all 3 G^3 's were readily ruthenated at N7 in the single-stranded DNA hexamer, only G^3 (or G^9) and G^6 , and not G^2 (G^8) were ruthenated in the free DNA duplex which is attributed to unfavorable steric interactions²² between the duplex and arene for binding at G^2 (G^8). The different ratios of **II-Ru-G³** : **II-Ru-G⁶** adducts in the reaction mixtures with Ru : **II** ratio of 1 : 1, indicates that there are differences in specificity from binding to internal bases or terminal nucleotides for the non-intercalator Ru-cym, the aromatic intercalator Ru-bip and non-aromatic intercalator Ru-tha. Little ruthenation of G^8 was observed in the mono-ruthenated duplexes, but the favorable binding sites were G^6 and G^{12} when di-ruthenated duplexes were reacted with $\{(\eta^6\text{-tha})\text{Ru}(\text{en})\}^{2+}$. These results also demonstrate that the combination of HPLC, ESI-MS together with 2D [^1H , ^1H] TOCSY NMR experiments is powerful for elucidating the selectivity of G-base ruthenation of the free duplex **II**, mono-ruthenated duplexes and di-ruthenated duplexes. Such knowledge of DNA interactions may be incorporated into design concepts for this class of anticancer agents and assist the exploration of structure-activity relationships.

The coordinative and penetrative intercalative interactions between Ru-tha and duplex DNA are different from that of DNA modified covalently by aromatic or bulky intercalators, in which the displacement or flip-out of bases near the modified sites may occur. Although both involve the modification of a DNA base *via* coordinative bonding, the penetrative intercalative interactions between Ru-tha and duplex DNA are also different from that of platinum complexes with an acridine side arm intercalator, where the threading intercalation does not cause helical bending. The $\text{C}-\text{H}\cdots\text{X}$ ($\text{X} = \text{O}$ or N) hydrogen bonds between protons of ring C of tha and O or N atoms of bases opposite the ruthenated nucleotides may contribute significantly to the intercalative interaction between Ru-tha and duplex DNA. The fact that penetrative intercalation has rarely been reported for mono-metallointercalators, implies that the direct Ru-N bonding may also assist with penetrative intercalation for the bulky tha ligand. Unwinding and distortion, while still maintaining the basic duplex structure, could contribute to the toxicity of the Ru-tha complex by hindering DNA repair. A bulky lesion is one of the six main DNA lesions that may invoke NER, for example, the first and rate-determining step in NER is the recognition of the bulky lesions by the XPC/HR23B protein heterodimer complex.⁶⁹ However, mutations and potentially cancer may result if the bulky lesions are resistant to NER.⁷⁰ The

high anticancer activity both *in vitro* and *in vivo* and the high potency of the tha complex may arise in part from the lack of repair of the lesions formed on DNA by this complex,²⁹ and assist with elucidation of structure–activity relationships for this class of complexes.

Acknowledgements

We thank the Wellcome Trust (Travelling Fellowship for HL), NSF (20871069) and JSSF (BK2008428) and facilities in the Edinburgh Protein Interaction Centre and Oncosense Ltd for their support for this work, Dr Haimei Chen for the gift of some of the complexes and colleagues in the EC COST Action D39 for stimulating discussions.

Notes and references

- 1 Y. K. Yan, M. Melchart, A. Habtemariam and P. J. Sadler, *Chem. Commun.*, 2005, 4764.
- 2 M. J. Clarke, *Coord. Chem. Rev.*, 2003, **236**, 209.
- 3 E. Alessio, G. Mestroni, A. Bergamo and G. Sava, *Curr. Top. Med. Chem.*, 2004, **4**, 1525.
- 4 P. J. Dyson, *Chimia*, 2007, **61**, 698.
- 5 J. E. Debreczeni, A. N. Bullock, G. E. Atilla, D. S. Williams, H. Bregman, S. Knapp and E. Meggers, *Angew. Chem., Int. Ed.*, 2006, **45**, 1580.
- 6 M. A. Jakupec and B. K. Keppler, *Curr. Top. Med. Chem.*, 2004, **4**, 1575.
- 7 F. Schmitt, P. Govindaswamy, G. Süß-Fink, W. Han Ang, P. J. Dyson, L. Juillerat-Jeanneret and B. Therrien, *J. Med. Chem.*, 2008, **51**, 1811.
- 8 P. M. Takahara, A. C. Rosenzweig, C. A. Frederick and S. J. Lippard, *Nature*, 1995, **377**, 649.
- 9 D. B. Zamble and S. J. Lippard, in *Cisplatin – Chemistry and Biochemistry of a Leading Anticancer Drug*, ed. B. Lippert, Wiley-VCH, New York, 1999, p. 73.
- 10 D. Wang and S. J. Lippard, *Nat. Rev. Drug Discovery*, 2005, **4**, 307.
- 11 B. E. Bowler and S. J. Lippard, *Biochemistry*, 1986, **25**, 3031.
- 12 W. J. Sundquist, D. P. Bancroft and S. J. Lippard, *J. Am. Chem. Soc.*, 1990, **112**, 1590.
- 13 L. Maresca, C. Pacifico, M. C. Pappadopoli and G. Natile, *Inorg. Chim. Acta*, 2000, **304**, 274.
- 14 J. R. Choudhury and U. Bierbach, *Nucleic Acids Res.*, 2005, **33**, 5622.
- 15 K. E. Erkkila, D. T. Odum and J. K. Barton, *Chem. Rev.*, 1999, **99**, 2777.
- 16 L. M. Wilhelmsson, F. Westerlund, P. Lincoln and B. Norden, *J. Am. Chem. Soc.*, 2002, **124**, 12092.
- 17 A. Greguric, G. I. Greguric, T. W. Hambley, J. R. Aldrich-Wright and J. G. Collins, *J. Chem. Soc., Dalton Trans.*, 2002, 849.
- 18 U. Schatzschneider and J. K. Barton, *J. Am. Chem. Soc.*, 2004, **126**, 8630.
- 19 M. Kang, A. Chouai, H. T. Chifotides and K. R. Dunbar, *Angew. Chem., Int. Ed.*, 2006, **45**, 6148.
- 20 C. Gossens, I. Tavernelli and U. Rothlisberger, *J. Am. Chem. Soc.*, 2008, **130**, 10921.
- 21 P. C. A. Bruijninx and P. J. Sadler, *Curr. Opin. Chem. Biol.*, 2008, **12**, 197.
- 22 H. K. Liu, F. Y. Wang, J. A. Parkinson, J. Bella and P. J. Sadler, *Chem.–Eur. J.*, 2006, **12**, 6151.
- 23 H. K. Liu, S. J. Berners-Price, F. Y. Wang, J. A. Parkinson, J. J. Xu, J. Bella and P. J. Sadler, *Angew. Chem., Int. Ed.*, 2006, **45**, 8153.
- 24 R. E. Morris, R. E. Aird, P. D. Murdoch, H. M. Chen, J. Cummings, N. D. Hughes, S. Parsons, A. Parkin, G. Boyd, D. I. Jodrell and P. J. Sadler, *J. Med. Chem.*, 2001, **44**, 3616.
- 25 R. E. Aird, J. Cummings, A. A. Ritchie, M. Muir, R. E. Morris, H. M. Chen, P. J. Sadler and D. I. Jodrell, *Br. J. Cancer*, 2002, **86**, 1652.
- 26 O. Novakova, H. M. Chen, O. Vrana, A. Rodger, P. J. Sadler and V. Brabec, *Biochemistry*, 2003, **42**, 11544.
- 27 H. M. Chen, J. A. Parkinson, R. E. Morris and P. J. Sadler, *J. Am. Chem. Soc.*, 2003, **125**, 173.
- 28 H. M. Chen, J. A. Parkinson, S. Parsons, R. A. Coxall, R. O. Gould and P. J. Sadler, *J. Am. Chem. Soc.*, 2002, **124**, 3064.
- 29 O. Novakova, J. Kasparkova, V. Bursova, C. Hofr, M. Vojtiskova, H. M. Chen, P. J. Sadler and V. Brabec, *Chem. Biol.*, 2005, **12**, 121.
- 30 H. M. Chen, J. A. Parkinson, O. Novakova, J. Bella, F. Y. Wang, A. Dawson, R. Gould, S. Parsons, V. Brabec and P. J. Sadler, *Proc. Natl. Acad. Sci. U. S. A.*, 2003, **100**, 14623.
- 31 M. Castellano-Castillo, H. Kostrhunova, V. Marini, J. Kasparkova, P. J. Sadler, J. M. Malinge and V. Brabec, *J. Biol. Inorg. Chem.*, 2008, **13**, 993.
- 32 C. Lian, H. Robinson and A. H. J. Wang, *J. Am. Chem. Soc.*, 1996, **118**, 8791.
- 33 K. W. Jennette, S. J. Lippard, G. A. Vassiliades and W. R. Bauer, *Proc. Natl. Acad. Sci. U. S. A.*, 1974, **71**, 3839.
- 34 W. I. Sundquist and S. J. Lippard, *Coord. Chem. Rev.*, 1990, **100**, 293.
- 35 B. P. Hudson and J. K. Barton, *J. Am. Chem. Soc.*, 1998, **120**, 6877.
- 36 J. G. Collins, R. M. Rixon and J. R. Aldrich-Wright, *Inorg. Chem.*, 2000, **39**, 4377.
- 37 L. Gonzalez-Bulnes and J. Gallego, *J. Am. Chem. Soc.*, 2009, **131**, 7781.
- 38 J. Tan, N. E. Geacintov and S. Broyde, *J. Am. Chem. Soc.*, 2000, **122**, 3021.
- 39 A. J. Danford, D. Wang, Q. Wang, T. D. Tullius and S. J. Lippard, *Proc. Natl. Acad. Sci. U. S. A.*, 2005, **102**, 12311.
- 40 F. Coste, J.-M. Malinge, L. Serre, W. Shepard, M. Roth, M. Leng and C. Zelwer, *Nucleic Acids Res.*, 1999, **27**, 1837.
- 41 Z. Johar, A. Zahn, C. J. Leumann and B. Jaun, *Chem.–Eur. J.*, 2008, **14**, 1080.
- 42 N. E. Geacintov, M. Cosman, B. E. Hingerty, S. Amin, S. Broyde and D. J. Patel, *Chem. Res. Toxicol.*, 1997, **10**, 111.
- 43 M. Lukin and C. de Los Santos, *Chem. Rev.*, 2006, **106**, 607.
- 44 I. Gomez-Pinto, E. Cubero, S. G. Kalko, V. Monaco, G. van der Marel, J. H. van Boom, M. Orozco and C. Gonzalez, *J. Biol. Chem.*, 2004, **279**, 24552.
- 45 K. Brown, B. E. Hingerty, E. A. Guenther, V. V. Krishnan, S. Broyde, K. W. Turteltaub and M. Cosman, *Proc. Natl. Acad. Sci. U. S. A.*, 2001, **98**, 8507.
- 46 Y. Cai, D. J. Patel, N. E. Geacintov and S. Broyde, *J. Mol. Biol.*, 2007, **374**, 292.
- 47 F. A. Tanius, S. F. Yen and W. D. Wilson, *Biochemistry*, 1991, **30**, 1813.
- 48 D. Sun, M. Hansen and L. Hurley, *J. Am. Chem. Soc.*, 1995, **117**, 2430.
- 49 H. Baruah and U. Bierbach, *Nucleic Acids Res.*, 2003, **31**, 4138.
- 50 Y. J. Chu, S. Sorey, D. W. Hoffman and B. L. Iverson, *J. Am. Chem. Soc.*, 2007, **129**, 1304.
- 51 Y. J. Chu, D. W. Hoffman and B. L. Iverson, *J. Am. Chem. Soc.*, 2009, **131**, 3499.
- 52 M. A. Nazif, J. A. Bangert, I. Ott, R. Gust, R. Stoll and W. S. Sheldrick, *J. Inorg. Biochem.*, 2009, **103**, 1405.
- 53 J. X. Dai, C. PUNCHIHewa, P. Mistry, A. T. Ooi and D. Z. Yang, *J. Biol. Chem.*, 2004, **279**, 46096.
- 54 H. Baruah and U. Bierbach, *J. Biol. Inorg. Chem.*, 2004, **9**, 335.
- 55 R. Guddneppanavar, G. Saluta, G. L. Kucera and U. Bierbach, *J. Med. Chem.*, 2006, **49**, 3204.
- 56 H. Baruah, M. W. Wright and U. Bierbach, *Biochemistry*, 2005, **44**, 6059.
- 57 S. Takenaka, *Bull. Chem. Soc. Jpn.*, 2001, **74**, 217.
- 58 W. A. Kibbe, *Nucleic Acids Res.*, 2007, **35**, W43.
- 59 J. Vinje, J. A. Parkinson, P. J. Sadler, T. Brown and E. Sletten, *Chem.–Eur. J.*, 2003, **9**, 1620; J. L. Beck, R. Gupta, T. Urathamakul, N. L. Williamson, M. M. Sheil, J. R. Aldrich-Wright and S. F. Ralph, *Chem. Commun.*, 2003, 626; J. A. Parkinson, Y. Chen, P. D. Murdoch, Z. J. Guo, S. J. Berners-Price, T. Brown and P. J. Sadler, *Chem.–Eur. J.*, 2000, **6**, 3636; D. R. Hare, D. Wemmer, S. H. Chou, G. Drobny and B. R. Reid, *J. Mol. Biol.*, 1983, **171**, 319.
- 60 S. L. Lam and S. C. F. Au-Yeung, *J. Mol. Biol.*, 1997, **266**, 745.
- 61 Y. Kwon, Z. Xi, L. S. Kappen, I. H. Goldberg and X. Gao, *Biochemistry*, 2003, **42**, 1186; G. Hwang, G. B. Jones and I. H. Goldberg, *Biochemistry*, 2004, **43**, 641.
- 62 E. Alessio, Y. Xu, S. Cauci, G. Mestroni, F. Quadrioglio, P. Viglino and L. G. Marzilli, *J. Am. Chem. Soc.*, 1989, **111**, 7068.
- 63 M. D. Reily and L. G. Marzilli, *J. Am. Chem. Soc.*, 1986, **108**, 8299.

-
- 64 V. M. Rodriguez-Bailey and M. J. Clarke, *Inorg. Chem.*, 1997, **36**, 1611.
- 65 A. Mukherjee, R. Lavery, B. Bagchi and J. T. Hynes, *J. Am. Chem. Soc.*, 2008, **130**, 9747; M. J. L. Cocco, L. A. Hanakahi, M. D. Huber and N. Maizels, *Nucleic Acids Res.*, 2003, **31**, 2944; Y. Coppel, J. F. Constant, C. Coulombeau, M. Demeunynck, J. Garcia and J. Lhomme, *Biochemistry*, 1997, **36**, 4831; W. D. Wilson, Y. Li and J. M. Veal, in *Advances in DNA Sequence Specific Agents*, ed. L. H. Hurley, Elsevier, New York 1992, p. 89; J. Lee, V. Guelev, S. Sorey, D. W. Hoffman and B. L. Iverson, *J. Am. Chem. Soc.*, 2004, **126**, 14036; X. G. Liang, H. Asanuma, H. Kashida, A. Takasu, T. Sakamoto, G. Kawai and M. Komiyama, *J. Am. Chem. Soc.*, 2003, **125**, 16408.
- 66 K. Wuthrich, *NMR of Proteins and Nucleic Acids*, John Wiley and Sons, Inc., USA, 1986, p. 30.
- 67 K. Kobayashi, Y. Asakawa, Y. Kikuchi, H. Toi and Y. Aoyama, *J. Am. Chem. Soc.*, 1993, **115**, 2648; K. Gkionis, J. A. Platts and J. G. Hill, *Inorg. Chem.*, 2008, **47**, 3893.
- 68 J. Sola, A. Riera, X. Verdaguer and M. A. Maestro, *J. Am. Chem. Soc.*, 2005, **127**, 13629; A. Uldry, J. M. Griffin, J. R. Yates, M. Pérez-Torrallba, M. D. Santa Maria, A. L. Webber, M. L. L. Beaumont, A. Samoson, R. M. Claramunt, C. J. Pickard and S. P. Brown, *J. Am. Chem. Soc.*, 2008, **130**, 945.
- 69 B. S. Thoma and K. M. Vasquez, *Mol. Carcinog.*, 2003, **38**, 1.
- 70 A. Luch, *Nat. Rev. Cancer*, 2005, **5**, 113; M. S. Greenblatt, W. P. Bennett, M. Hollstein and C. C. Harris, *Cancer Res.*, 1994, **54**, 4855.